Conf-950228--5
SAN095-0609C

Vibration control for precision manufacturing at Sandia National Laboratories

Terry Hinnerichs and David Martinez

Structural Dynamics and Vibration Control Department
Sandia National Laboratories
Albuquerque, NM 87185
(505) 844-9257 tdhinne@sandia.gov

ABSTRACT

Sandia National Laboratories performs R&D in structural dynamics and vibration suppression for precision applications in weapon systems, space, underwater, transportation and civil structures. Over the last decade these efforts have expanded into the areas of active vibration control and "smart" structures and material systems. In addition, Sandia has focused major resources towards technology to support weapon product development and agile manufacturing capability for defense and industrial applications. This paper will briefly describe the structural dynamics modeling and verification process currently in place at Sandia that supports vibration control and some specific applications of these techniques to manufacturing in the areas of lithography, machine tools and flexible robotics.

1.0 INTRODUCTION

Sandia National Laboratories performs R&D in structural dynamics and vibration suppression for applications in weapon systems and defense. Over the last decade these efforts have evolved into the areas of active vibration control and "smart" structures and material systems. In addition, Sandia has focused major resources to support weapon product development and advanced agile manufacturing technology for defense and industrial applications. This paper will discuss several projects in advanced vibration control for precision manufacturing systems. We will give an overview of ongoing and new-start projects at Sandia in chatter suppression in machine tools including tool/workpiece interaction characterization, vibration control in lithography machines, and flexible robotics. Many of these projects are collaborative efforts with private industry, universities, and other government agencies. Also, these projects involve many of the technical issues listed in the National Center for Manufacturing Sciences white paper including structural optimization for stiffness, magnetic levitation, non-linear model reduction, active and passive vibration control, and on-line structural system identification for robust adaptive controls and machine condition monitoring.

2.0 STRUCTURAL DYNAMICS MODELING AND VERIFICATION PROCESS

Structural dynamics modeling, computational simulation, and model verification are essential elements for manufacturing applications. Sandia has ongoing efforts to develop tools for simulation, as well as the related technologies of System Identification and optimization. These technologies involve integration of analytical and experimental structural dynamics. Originally developed for weapon and space structures, these techniques are now being applied to applications in manufacturing.

Computational modeling is the process of developing a mathematical simulation of a conceptual design. This typically involves finite element or boundary element models of structures and systems. Figure 1 shows two deformed finite element meshes representing two vibrational modes of the upper platten of a lithography machine. These models can be used for design verification, analysis, and optimization of the design. Optimization is a very computationally intensive process. Sandia is performing research into optimization methods for various disciplines of engineering science, including massively parallel computing applications.

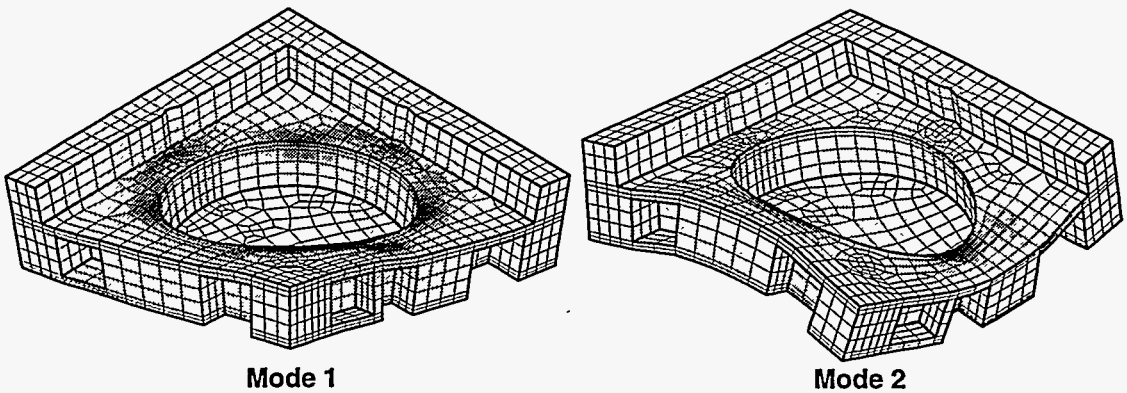

Figure (1): First and Second Flexible Mode Shape of a Lithography Platen/Mirror

DISCLAIMER

DISCLAIMER

Portions of this document may be illegible in electronic image products. Images are produced from the best available original document.

Structural dynamics analysis and model verification are essential elements for structural control. Sandia has an ongoing effort to develop both the model verification process, as well as specific analytical and experimental techniques for system identification. System identification is the process of obtaining a computational model from experimental data. In one of its simplest forms, mode shapes and frequencies are extracted from test data and used directly. In its more complicated form, system identification is an integration of analytical and experimental structural dynamics. It is an automated method for calibrating structural dynamics models (e.g. finite element models) with measured data, and accounts for the uncertainty in both the data and the physical parameters defining the model. Constrained optimization, genetic algorithms and Bayesian estimation procedures have been implemented at Sandia. The interaction of modeling with testing requires close coupling of experimental and analytical tools. Research in integrated analytical-experimental model verification requires extensive computational resources for both the estimation/optimization algorithms and the finite element function evaluation. These techniques become important for manufacturing applications where accurate simulations and virtual prototyping are required for overall system design and implementation of vibration control techniques.

3.0 ADVANCED LITHOGRAPHY TECHNOLOGY FOR MICROELECTRONIC MANUFACTURING

Sandia is developing active and passive vibration control methodologies for advanced lithography machines that print electrical circuits on silicon wafers. This precision printing step is a critical part of the microelectronics manufacturing process.

3.1 Active vibration control

This section presents a conceptual design[1] of a supplemental flexible body control system for a magnetically levitated platen used in the manufacture of integrated circuits (ICs). This work exemplifies the benefits of detailed modeling and simulation prior to fabricating system components.

Recently, a two stage positioning system which combines large travel capabilities and precision placement capabilities was developed for use in photolithography-based IC manufacturing. In this system, a coarse stage drives a fine stage through large travel distances (up to 200 mm) using motor driven ball screws, and the fine stage precisely maneuvers a wafer platen over a +/ - 250 μm range using electromagnetic actuators. The magnetically levitated platen exhibits six degree of freedom rigid body motion. This motion is controlled by a rigid body control system consisting of capacitive proximity sensors, nonlinear electromagnetic actuators, and Proportional-Derivative (PD) controllers. Since the platen is magnetically levitated, positioning limitations caused by friction, machining tolerance, and hysteresis are virtually eliminated. In recent tests, this two stage system consistently produced placement accuracies better than 10 nm.

As with many positioning systems, excitation of flexible body modes limits the achievable positioning speed. Active damping of the platen flexible body modes can permit increases in the rigid body controller bandwidth and, ultimately, IC production rates. To investigate the validity of this approach, a prototype platen incorporating Lead Zirconate Titanate (PZT) stack actuators for active vibration control has been designed. Actuators mounted flush with the platen top surface will be used to suppress the vibration of the first two modes with frequencies of 972 and 1619 Hz, respectively. The first two mode shapes with strain energy contours extracted from a finite element analysis are shown in Figure 1. Proper placement of PZT stacks for vibration suppression requires attention to both location and orientation. To facilitate actuator placement, a detailed simulation of the system based on the finite element model was developed. Three actuator placements were selected by monitoring normal strains on the platen surface during simulated maneuvers under the direction of the of the rigid body controller.

A local rate feedback control algorithm targeting the first two modes of vibration was designed and incorporated into the system simulation. A simulated transfer function from an electro-magnetic actuator to a capacitive sensor is shown in Figure 2 with the flexible body controller open and closed. The active damping provides approximately 30 db of attenuation in the first and second modes. This increased stability has the potential for permitting significant increases in the rigid body positioning speed as shown in Figure 3 for a simulated 10 μm step maneuver. Without the active vibration control, the bandwidth of the rigid body control loop is limited to approximately 30 Hz beyond which an instability is encountered. With active damping, this instability is not encountered until the bandwidth exceeds 125 Hz, and the positioning speed is greatly increased. As a result of this investigation, fabrication of the prototype platen has proceeded in order to experimentally demonstrate the benefits derived through active vibration control.

3.2 Passive vibration damping

In this section, a viscoelastic tuned-mass damper used to suppress specific structural modes of a prototype lithography platen is described[2]. As in the earlier section, the platen is magnetically levitated and it is repositioned and held in position by a closed-loop feedback control system. Of primary interest in the present work is the first and second natural modes of the platen, occurring at 1,250 Hz and 1970 Hz, respectively. The mode shapes for the test platen are similar to those shown for the active control experiment in Figure 1.

The strategy of tuned mass dampers (also known as vibration absorbers or frequency splitters) is to connect an additional mass to a structure using a spring whose stiffness is such that the frequency of that mass-spring system is identical to that of the original structure. For viscoelastic vibration absorbers, the connection between the added mass and the original structure is contrived to involve some damping when there is relative motion between the two. When the base structure resonates, the added mass will be excited to relative motion and not only will the structure be de-tuned to the original frequency, but some mechanical energy will be bled off through viscous dissipation.

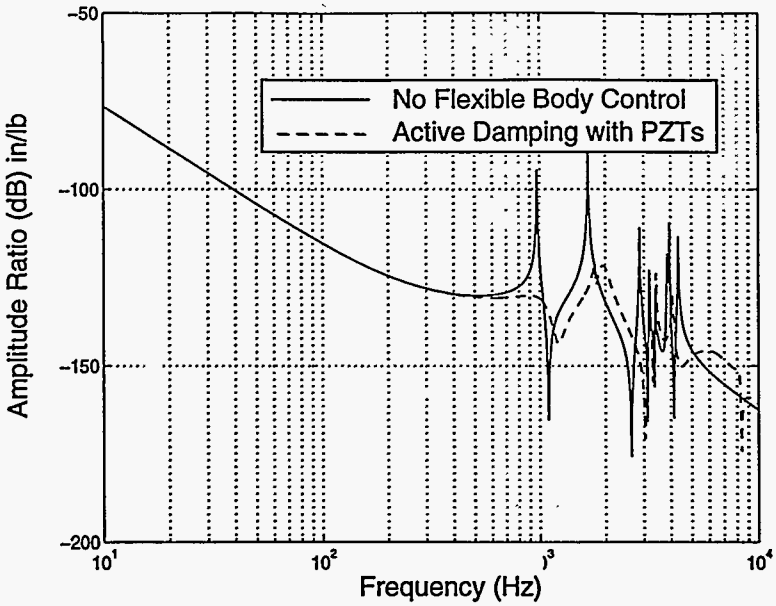

Figure (2): Sample Transfer Function With Effect of Flexible Body Control.

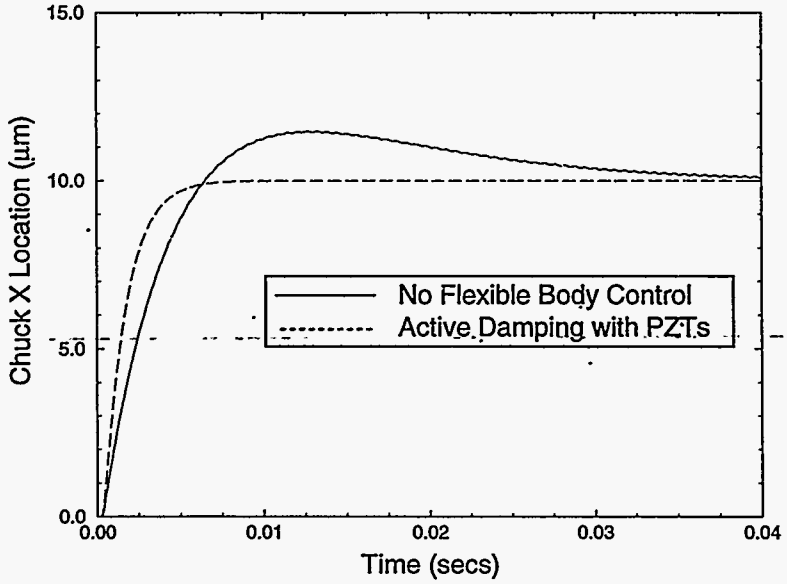

Figure (3): Comparison of Best Responses Obtained With and Without Flexible Body Control.

The viscoelastic dampers employed in this project were small masses sitting on thin pads of very lossy viscoelastic solid. The damped vibration absorber was chosen to function in an extensional mode. The masses used were brass (fairly dense, non-magnetic, and readily available) cylinders 1.25" diameter and 0.6" thick, weighing 0.23 lb. each. The viscoelastic material used was Scotch-Seal synthetic putty 1167. Computational modeling enabled the prediction of optimum thicknesses of Scotch-Seal over a range of excitation frequencies as verified by test data.

The effectiveness of the viscoelastic tuned mass dampers is best illuminated by experiments in which the platen was deliberately excited by white noise injected into the control system. A single 3-axis accelerometer mounted on a platen corner was used to obtain platen acceleration. The platen is shown in the lithography device in Figure 4. Two vibration absorbers tuned to the first natural frequency were put at antinodes of the first mode (i.e. corners) and two vibration absorbers tuned to the second natural frequency were placed at antinodes of the second mode (i.e. mid-sides). The results are indicated in Figure 5. We see that substantial vibration suppression - on the order of 20 db - are achieved for each mode. The results show that the tuned-mass

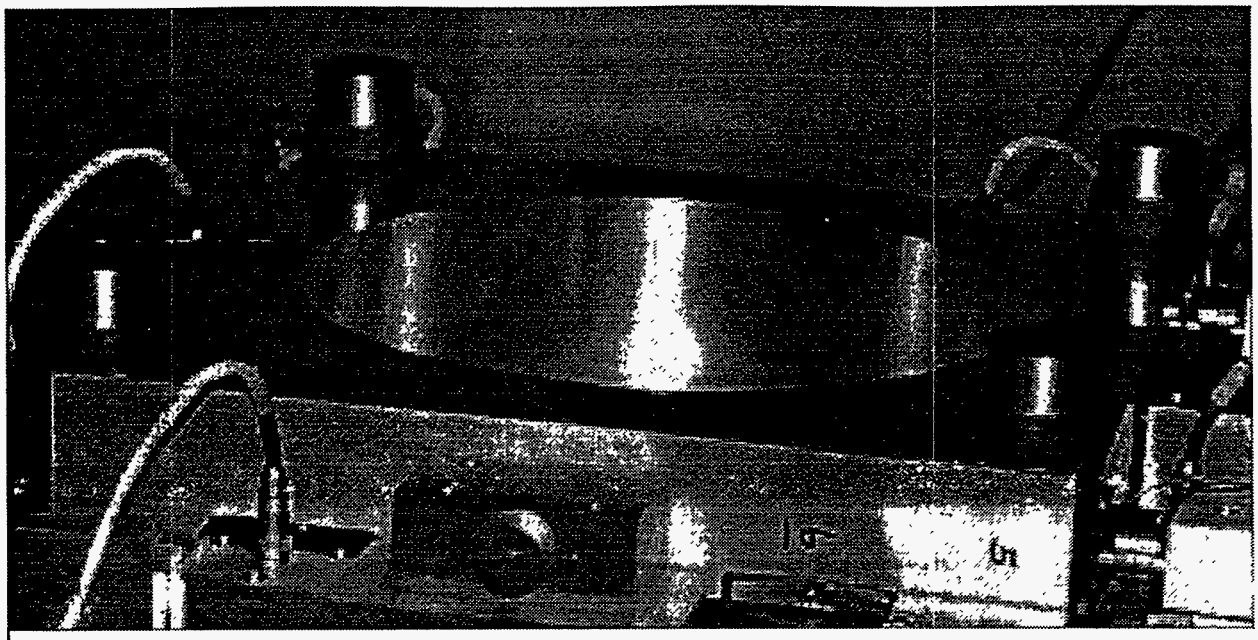

Figure (4): Platen Mounted on the Lithography Device with Viscoelastic Vibration Absorbers.

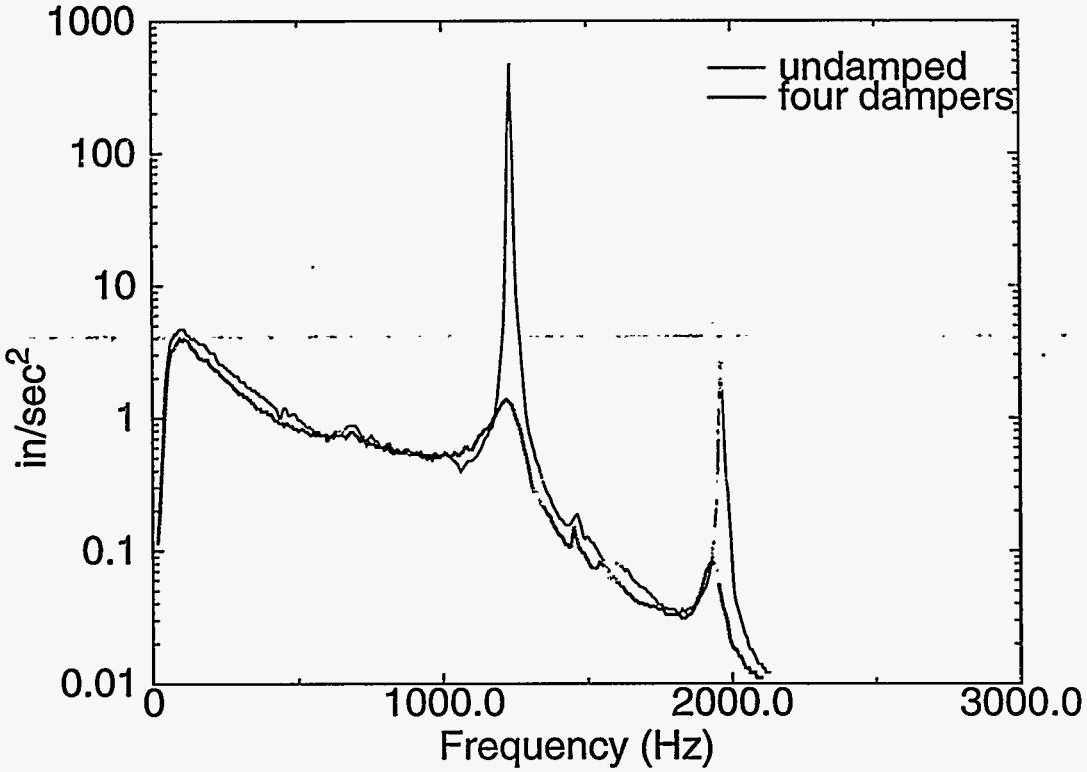

Figure (5): Acceleration spectral response of platen with damping on first and second mode.

dampers were successful in significantly reducing acceleration at the specific structural modes (first and second) of interest. As in the active control case, this permits extension of the rigid body controller bandwidth.

4.0 MODELING/SIMULATION FOR VIBRATION CONTROL OF HIGH SPEED MILLNG MACHINES[3]

This section describes the modeling and computational simulation developed for milling tool vibration based on recently published models of the cutting process[4-9]. This development was undertaken specifically to support our research in active

vibration control for machine tools. The Eigensystem Realization Algorithm is used to identify low order models of machine tool dynamics from experimental data[10-11].

4.1 Cutting model

The process of metal removal in milling couples the machine tool dynamics with the tangential and normal cutting forces generated at the tool-workpiece interface. Figure 6 shows a diagram of a milling tool passing through a workpiece. The inertial

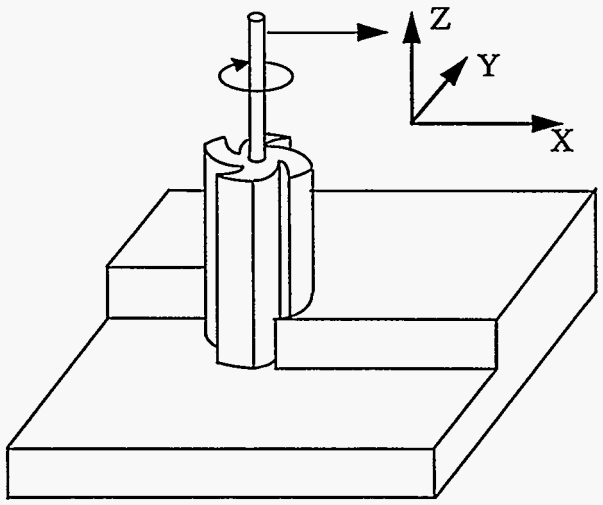

Figure (6): Schematic Diagram of Milling Cutter.

X axis is located along the direction of the feed with the Y axis lying in the plane. The Z axis is directed along the axis of the cutting tool with the rotation of the milling tool assumed to be along the negative Z axis. Ignoring the axial flexibility of the cutting tool, vibration of the cutting tool occurs in the X-Y plane. Driving point transfer functions containing all of the pertinent dynamics can be readily obtained experimentally by measuring the impulse response functions of the cutting tip. Then, a state space model of the form

$$\dot{\underline{x}}(t) = A\underline{x}(t) + B\underline{f}(t) \tag{1}$$

$$\underline{y}(t) = C\underline{x}(t) + D\underline{f}(t) \tag{2}$$

can be generated using the Eigensystem Realization Algorithm[10-11]. In Equation 1 and Equation 2, A, B, C, D are the state space matrices, $\underline{x}(t)$ is the n dimensional state vector, $\underline{f}(t) = \left[f_x(t)\ f_y(t)\right]^T$ is the input vector of cutting forces, and $\underline{y}(t) = \left[X(t)\ Y(t)\right]^T$ is the vector of tip displacements along the X and Y axes. The cutting forces are based on previously published models in which tool vibrations are recorded on the workpiece surface[8]. As shown in Figure 7, previous vibrations excite current vibrations by altering the instantaneous chip thickness.

4.2 Sample Tool Analysis

This section describes a stability analysis for a Giddings and Lewis Horizontal Boring Mill located at Sandia. The Boring Mill's 2 inch diameter 4 tooth cutting tool is shown in Figure 8. Two accelerometers were mounted approximately ninety degrees apart and driving point transfer functions were measured for a variety of head rotations and quill lengths. For each test, the transfer functions were computed from an average of ten impulse responses generated from strikes from an instrumented hammer.

A driving point transfer function and an impulse response function are shown in Figure 9. The impulse response function was obtained by an inverse Fast Fourier Transform of the frequency response function. The vibration of the tool tip was dominated by two lightly damped modes at 200 and 700 Hz. This data was fit using the Eigensystem Realization Algorithm[10-11], producing a fourth order model that closely matched the frequency response function shown in Figure 9.

Although the subject boring mill has a maximum speed of 500 rpm, the simulation is run at higher speeds to clearly illustrate the classical stability lobes. An estimated stability diagram for this configuration for a full immersion slotting cut on aluminum is shown in Figure 10. A 40 by 40 grid of data points was generated with the cutting speed ranging from 1000 to 30000 rpm and the axial depth of cut ranging from 0.1 to 4.5 mm. For all data points, the feed rate was set at 100 mm/sec and the cutting was simulated for 30 revolutions. The vibration amplitude contours indicate the presence of the classic stability lobes with the lobes becoming more concentrated in the low speed range. Considering a 20 μm peak to peak vibration amplitude, a tool speed of 10,000 rpm offers the potential for higher metal removal rates than at 20,000 rpm. Note that at the highly stable speeds of 3000

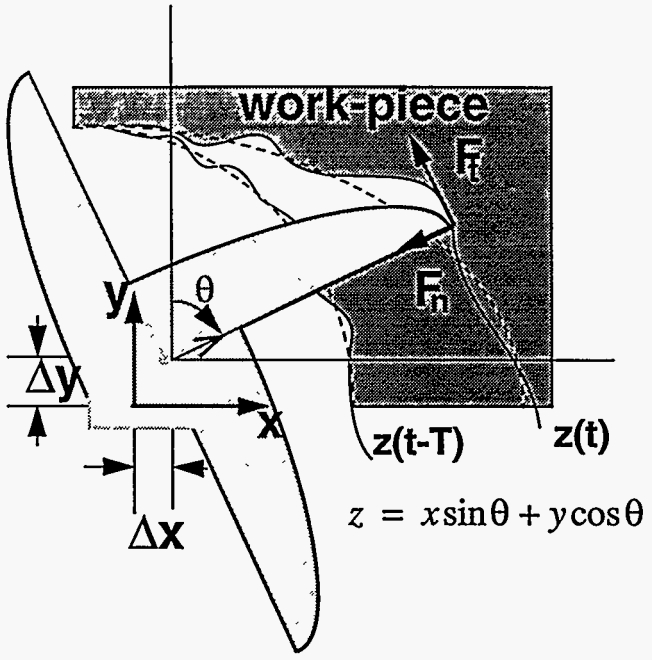

Figure (7): The Regeneration of Waviness.

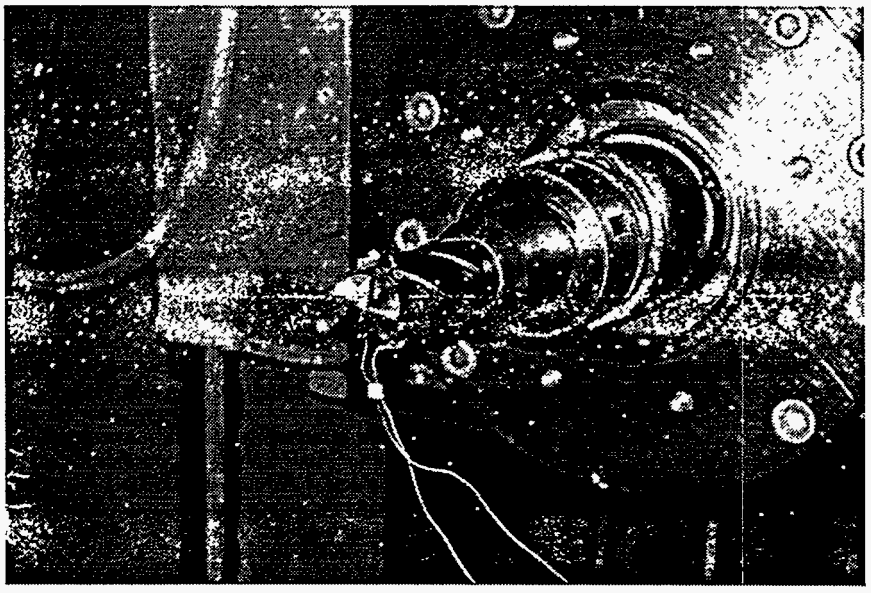

Figure (8): Milling Tool with Attached Accelerometers.

and 10,000 rpm, the tooth passing frequencies are approximately equal to the natural frequencies of the first and second modes, respectively. These stability pockets have been the focus of much research on high speed machining[7].

4.3 Estimated Surface Finish

In this section, estimated surface finish is presented based on simulation results. With the tool speed at 5000 rpm, the cutting depth was first set to 0.5 mm. According to Figure 10, these parameters established a relatively stable cutting condition. The simulated surface finish of the workpiece is illustrated in Figure 11. The workpiece surface finish was estimated by plotting the inertial paths of each of the cutting teeth. As a consequence of the stable cutting conditions a smooth surface finish was produced. However, increasing the depth of cut to 1.5 mm produced a relatively unstable cutting condition as illustrated by Figure 10. The surface finish for this cutting condition is shown in Figure 12. The surface is characteristic of chatter vibrations. In some scenarios, chatter vibrations can lead to tool breakage and damage to the machine as well as the workpiece. Therefore, the focus of this work is to develop active vibration control strategies that can mitigate chatter effects.

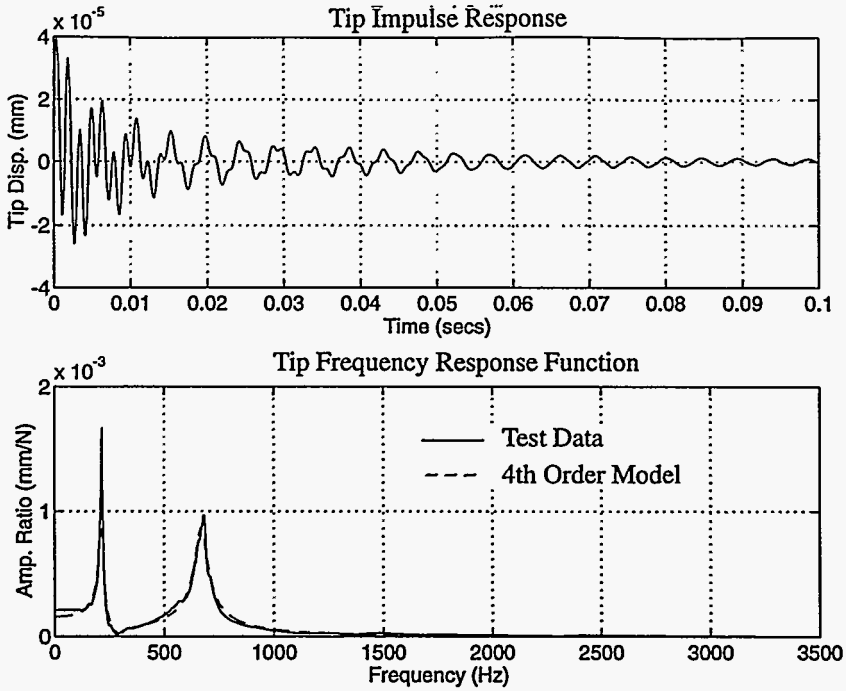

Figure (9): Milling Machine Dynamics Summary

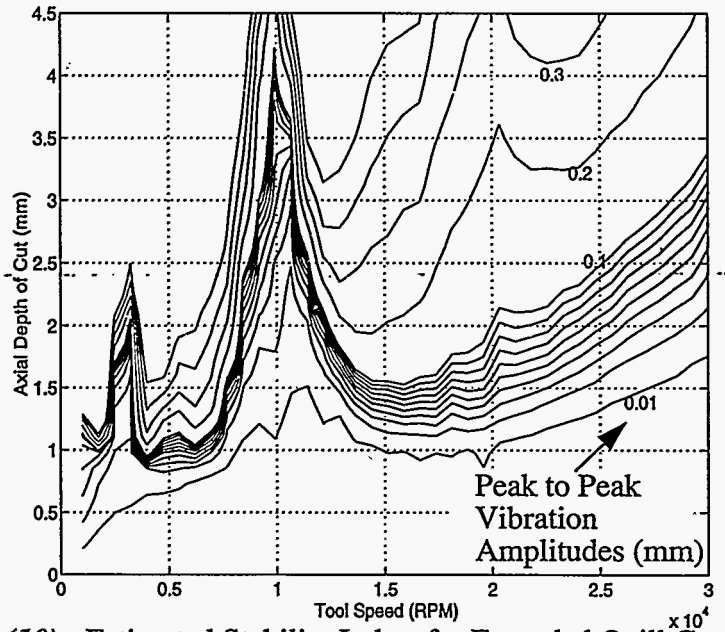

Figure (10): Estimated Stability Lobes for Extended Quill Configuration

5.0 FLEXIBLE ROBOTICS

Procedures for trajectory planning and control of flexible link robots are becoming increasingly important to satisfy performance requirements in manufacturing as well as in the case of hazardous waste removal efforts. In this Flexible Robotics section brief descriptions of recent work at Sandia will be given on Input Shaping, Dynamic programming, Recursive Quadratic Programming, and Sliding Mode Control applied to robotic control.

5.1 Input Shaping

In this section applications of input shaping to flexible link robotics and industrial cranes is discussed. A brief description of the methods employed for generating shaped inputs is presented along with experimental verification results for specific systems.

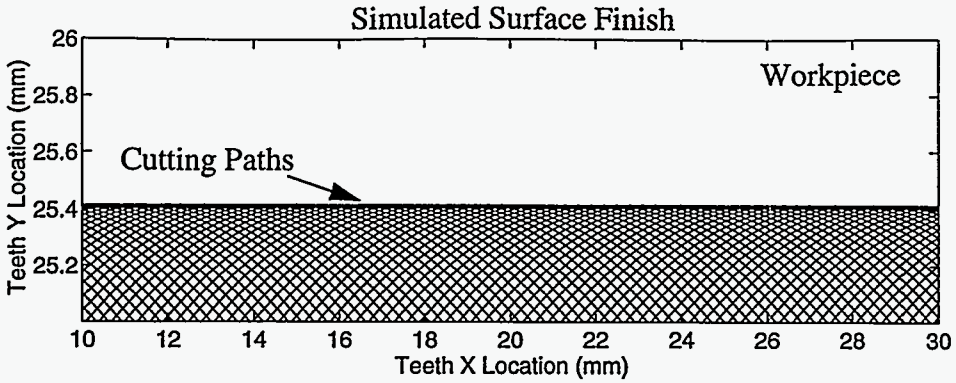

Figure (11): Cutting Simulation for Extended Quill, N=5000 rpm, b=0.5 mm.

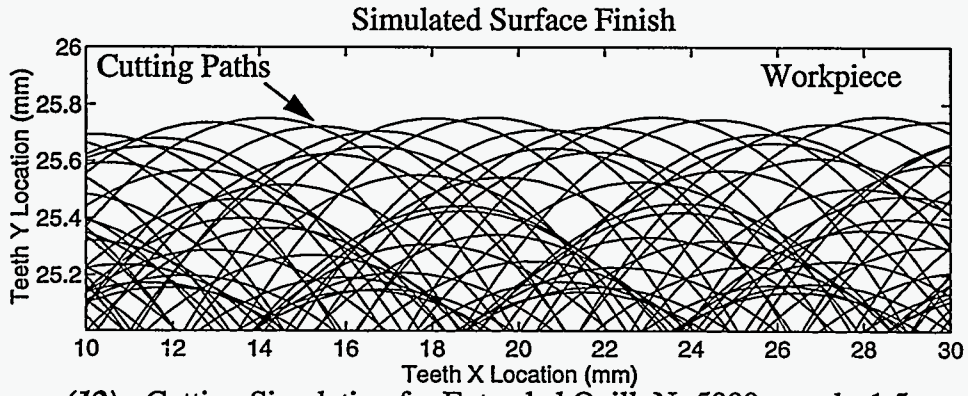

Figure (12): Cutting Simulation for Extended Quill, N=5000 rpm, b=1.5 mm.

In general, input shaping can be described as the generation or alteration of open-loop system inputs to achieve a desired system output. For the examples considered here, the shaped input is parameterized by a set of basis functions. Coefficients of these basis functions are determined via a numerical optimization process by minimizing a specific cost function of interest. Typically, the cost function is a measure of residual vibration of a payload. For the case of the flexible robot the payload is at the end of a flexible arm. For the crane example, the payload is at the end of a pendulum-like payload line.

The first example of input shaping explored at Sandia[12] concerned the slewing of a flexible rod in the horizontal plane. It is well known that both vertical and horizontal modes of oscillation are excited when this type of maneuver is performed in a gravitational field. It was shown analytically and verified experimentally that a hub angular acceleration pulse profile could be used to yield residual oscillation free slewing of the rod. A typical pulse profile is shown in Figure 13. This profile is parameterized uniquely by the three quantities A the pulse amplitude, T_w the pulse duration and t_c the coast time between

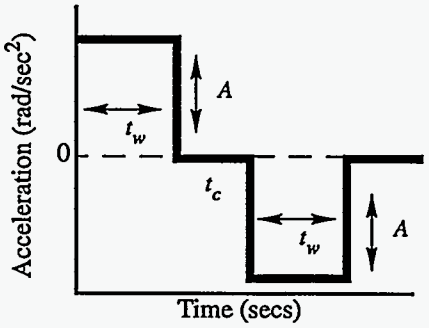

Figure (13): Acceleration Profile

pulses. Using a simulation of the system equations of motion in conjunction with a numerical optimization code, theses parameters are easily obtained by minimizing a cost function representative of the residual rod vibration.

The example described above was verified using a D.C. motor driven system, consisting of a light weight rod. Having performed this proof-of-concept study, the next step involved application of input shaping using an industrial-type robot[13]. To this end, the Sandia Heavy-Lift Hydraulic Robot was used. Although this system utilizes a novel U-Joint configuration for obtaining two rotational degrees of freedom at each joint, only one axis of rotation was employed. A flexible rod with tip mass was attached to the first link of the robot as shown in Figure 14. The symmetric maneuvers considered began at some angle $-\theta_c$ passing through

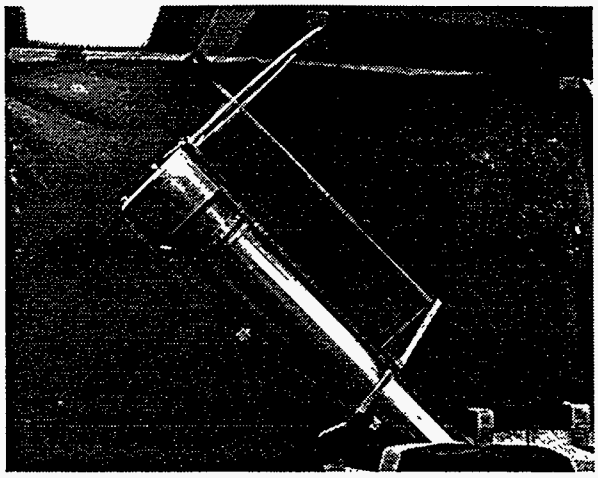

Figure (14): Sandia's Heavy-Lift Hydraulic Robot with Attached Flexible Rod.

the vertical position to a final angle of θ_c. At the end of the maneuver the tip mass was to be residual oscillation free. Although the equations of motion for this system were different than the horizontal slew described previously, a smoothed version of the hub angular acceleration pulse profile of Figure 13 was used. An added complexity involved accurate modeling of the hydraulic joint actuator dynamics. However, input shaping again was successfully demonstrated experimintally after obtaining accurate model for both the flexible rod and the hydraulic actuator. Figure 15 shows experimental data obtained via an accelerometer

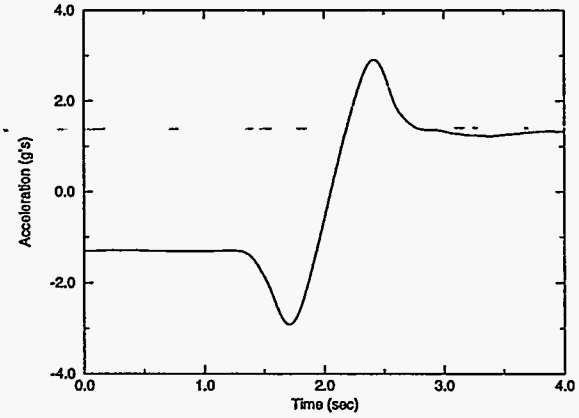

Figure (15): Filter In-Plane Accelerometer Data

placed on the tip mass. The initial and final nonzero acceleration is due to the gravitational field. At the completion of the maneuver, at approximately 3.0 seconds, the tip mass is seen to be residual oscillation free.

The last example discussed here concerns point-to-point payload positioning using a rotary jib crane[14]. Again, although the equations of motion were significantly different from the previous two cases, it was shown that a similar hub acceleration profile would yield residual oscillation free maneuvers. Situations involving fixed and variable load-line length were experimentally verified. Furthermore, it was also shown that residual oscillation specified maneuvers could be performed using the same input shaping technique. For these cases the cost function minimized for obtaining input shape parameters was modified to measure only the residual oscillation to be suppressed.

Continued work in this area is ongoing at Sandia not only in the area of robotics and industrial cranes, but also in problems involving reorientation of satellites with flexible appendages.

5.2 Robot Trajectory Planning via Dynamic Programming[15]

In this section results are given for applying the method of dynamic programming to rest-to-rest maneuvers of a single-link robot with a flexible payload. The dynamic programming approach is applicable to rigid, flexible, and redundant robots.

A sketch of the model showing the relevant parameters is given in Figure 16. For this example, the optimal rest-to-rest trajectory

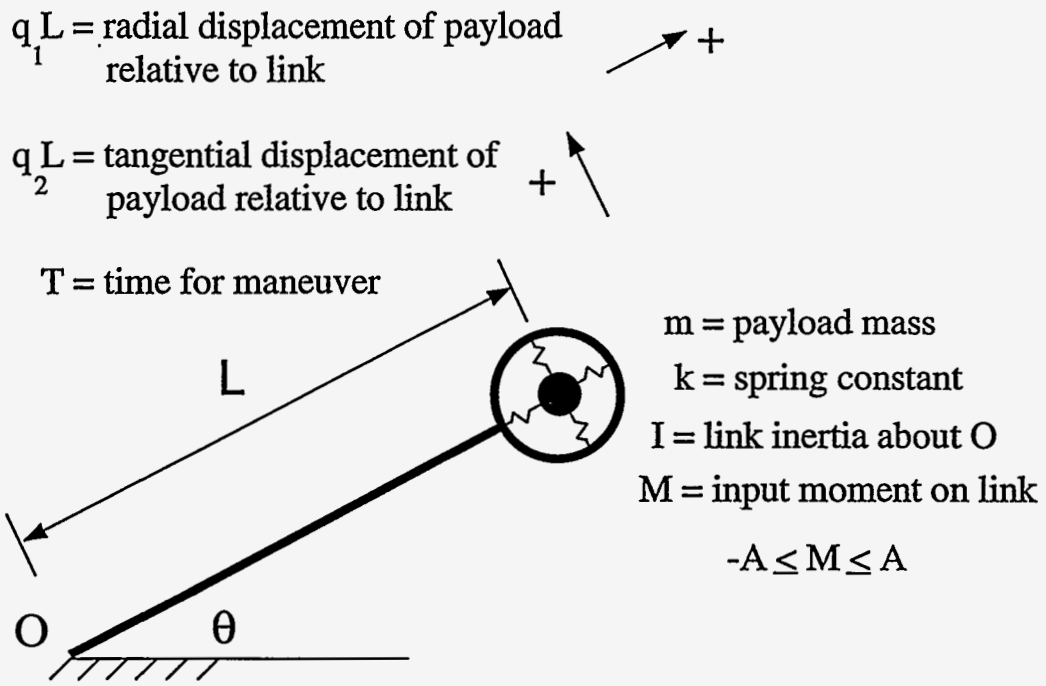

Figure (16): Sketch of Single-Link Manipulator with a Flexible Payload.

is defined as the one which minimizes the summation of the square of the input moments for each time step. Since closed-form solutions of this type of problem are generally not available, the dynamic programming algorithm made use of a fourth-order Runge-Kutta numerical integration scheme.

Results presented in Figure 17 show the states and inputs as functions of nondimensional time τ. The symmetries of the inputs and states about the time midpoint are evident in the figure. The effect of varying payload stiffness, C_3, on the optimum torque profile is also shown in Figure 17. C_3 is the square of the natural frequency of the payload mass times the maneuver time squared and u is the applied nondimensional moment equal to M/A. Results are presented for the two values of C_3. As C_3 is increased, the torque profile approaches the one for a rigid payload. As C_3 decreases, a critical value is reached below which the rest-to-rest maneuver is not possible. This lower bound is an important constraint to consider for the control of flexible payloads where the final angle and final time are specified.

This method for trajectory planning shows much promise. Additional testing and evaluation will be required, however, to assess more completely its strengths and limitations.

5.3 Optimal Trajectories for Flexible-Link Manipulator Slewing Using Recursive Quadratic Programming[16]

In this section a numerical optimization process, using an experimentally verified modal model, is used for obtaining minimum time joint torque and angle histories. The optimal joint states are used as commands to the proportional-derivative servo actuated joints. It has been shown that utilizing link flexibility in designing open loop joint commands can result in improved performance as opposed to damping vibration throughout a trajectory. The efficient use of link compliance is exploited in this work. Specifically, experimental verification of minimum time, straight line tracking using a two-link planar flexible robot is presented.

5.3.1 Experimental set-up

The two-link robot of Figure 18 consists of two flexible aluminum links, two motor amplifiers, two DC servo motors, two joint angle encoders, two joint angle tachometers and a VME bus computer system. The flexible links are mounted so as not to produce significant deformation in the vertical direction. The motors at joints one and two will be referred to as the hub and elbow joints from here on.

5.3.2 The structural model

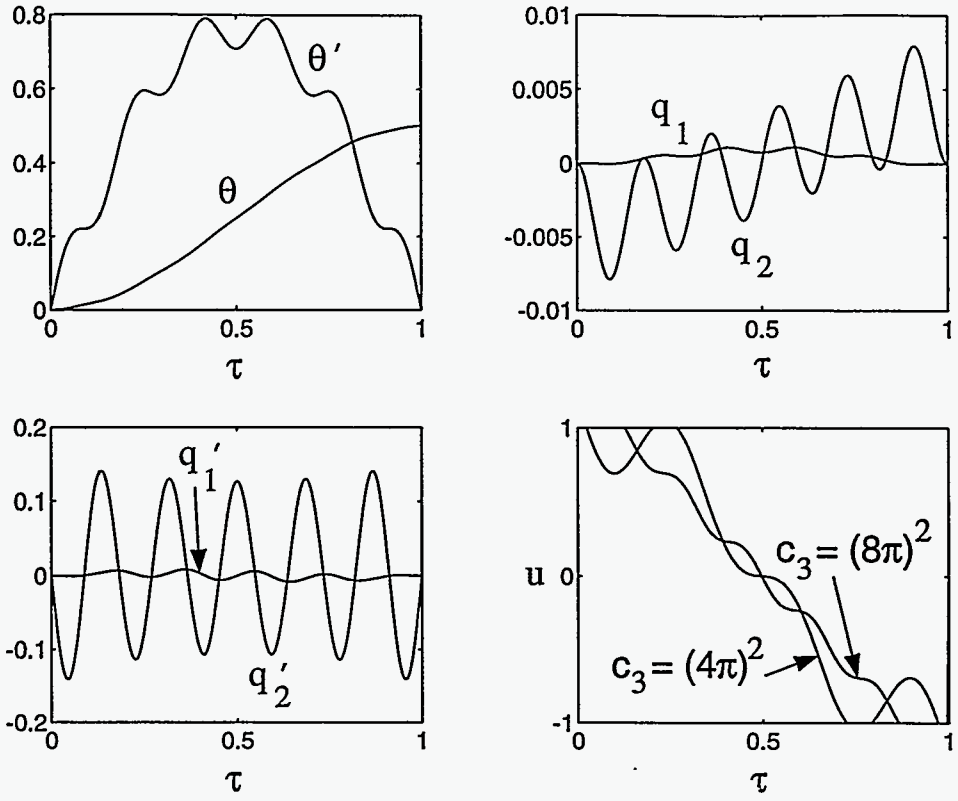

Figure (17): Rest-to-Rest Motion of Single-Link Manipulator with a Flexible Payload.

Figure (18): Sandia Flexible Two-Link Robot

All motion is assumed to occur in the x-y plane as shown in Figure 19. The center of each cross section is identified by its arc length distance from the hub s. The vector $\beta(s, t)$ is the unit tangent along the arm at s, and θ is the inertial angle to β. Each flexible link is discretized into three elements, furthermore each rigid link/joint mounting bracket is described by a single element. The elbow joint is described by two collocated nodes so that a nonzero angle is permitted. The constraint of continuous slope between angles is satisfied by the choice of element basis functions. Hamilton's principle is applied to the discretized system after obtaining expressions for kinetic energy, strain energy, and the virtual work due to the applied motor torques. The result is a set of second-order equations in the node unknowns, $\dot{\theta}_n$

$$\hat{k} \cdot \tau_m(t) = \sum_{n=1}^{nodes} \left[\gamma_m(t) \cdot \gamma_n(t) \ddot{\theta}_n(t) M_{m,n} - \left(\gamma_m(t) \cdot \beta_n(t) (\dot{\theta}_n(t))^2 M_{m,n} + \gamma_m(t) \cdot \beta_n(t) K_{m,n} \right) \right] \quad (3)$$

where $\hat{k}$ is the z-axis unit vector, τ_m is the applied torque at node m, γ_m is a unit orthogonal vector at node m, θ_m is the inertial angle at node m, $M_{m,n}$ and $K_{m,n}$ are the mass and stiffness matrices, respectively, and β_m is the unit tangent vector at node m. The equations of motion of Eq. () are integrated using a Newmark-β method. The solutions of the resulting nonlinear algebraic equations in $\ddot{\theta}_n$ are obtained with a Newton method.

The structural model was updated based on modal testing of the structure. However, due to the accuracy of the original model, the updated model gives nearly identical results.

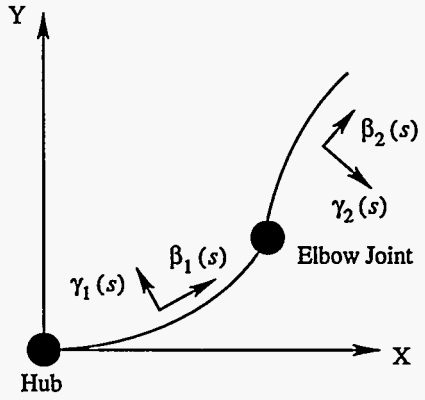

Figure (19): Coordinate System Definition

5.3.3 Optimal trajectory planning

Minimum-time, straight line tip trajectories are considered here. Constraints on these trajectories are: completing a rest-to-rest maneuver, tracking a specified path $(x(t), y(t))_{tip}$, slewing between specified endpoints $[(x(t_o), y(t_o)), (x(t_f), y(t_f))]_{tip}$, and not exceeding actuator torque limits, $\pm\tau_i$. End constraints on both velocities and accelerations are required to drive the flexible structure to rest at the final time t_f. Torque limits are incorporated naturally into the controls as

$$\tau_i = |\tau_{imax}| \sin\alpha_i(t) \quad (4)$$

where $\alpha_i(t)$ are free variables. Assuming the configuration initially starts at rest, the optimization problem can be stated as:

minimize: $J = t_f - t_0$
subject to:--input actuator torques, τ_i
--the finite element model
--known initial conditions
and constrained by Equation 5:

$$C = \begin{bmatrix} x_{tip}(t_f) - x_{specified}(t_f) \\ y_{tip}(t_f) - y_{specified}(t_f) \\ \dot{\theta}_1(t_f) \\ \dot{\theta}_2(t_f) \\ \ddot{\theta}_1(t_f) \\ \ddot{\theta}_2(t_f) \\ \int_0^{t_f} [y_{tip}(x_{tip}(t)) - y_{line}(x_{tip}(t))]^2 \, dt \end{bmatrix} = 0 \quad (5)$$

where $y_{tip}(x_{tip}(t))$ is the Y-axis coordinate of the second link tip corresponding to the X-axis tip coordinate at the current time, t. Note that the tip-tracking criterion includes an integral constraint for following the line and a point constraint for acquiring the end condition, while the constraints needed to bring the structure to rest are simply point constraints. No constraint is placed on link vibration during slew maneuvers and the structure is allowed to vibrate during the trajectory.

5.3.4 Servo dynamics and input command conditioning

The joint actuators consist of D.C. motors and current regulating amplifiers. Under the assumption that current is proportional to motor torque, the actuators are torque following devices. As a first step to achieving the tracking objective, the joint torques, as calculated by the optimization process, are used as sole inputs to the current regulating amplifiers. The equation of motion describing the dynamics of this system are

$$J_m\ddot{\theta}_m + B_m\dot{\theta}_m = K_i i_a - \tau_L \tag{6}$$

where J_m is the motor inertia, B_m is the motor viscous friction damping, K_i is the motor torque constant, i_a is the motor armature current, τ_L is the nonlinear load torque function imparted to the motors due to the motion of the links, including deformation degrees of freedom, and θ_m is the joint angle. Because the dynamics of Eq. (6) are not included in the optimization process described in the previous section, the optimal torque (current) commands result in tracking errors in excess of 11 cm as shown in Figure 20.

The next step is to implement Proportional-Derivative (PD) servo loops at each joint's D.C. motor actuator. The control law at each joint takes the form

$$K_i i_a = K_p(\theta_c - \theta_m) + K_D(\dot{\theta}_c - \dot{\theta}_m) \tag{7}$$

where K_P is the proportional gain, K_D is the derivative gain, and θ_c is the commanded joint angle. The equation of motion describing the dynamics of the servo controlled system are

$$J_m\ddot{\theta}_m + (B_m + K_D)\dot{\theta}_m + K_P\theta_m = K_D\dot{\theta}_c + K_P\theta_c - \tau_L \tag{8}$$

In this case the joint angle commands and joint angular velocity commands obtained from the optimization process are used as inputs to the servo controlled joint actuators. The performance of this method suffers from the lack of compensation of the dynamic effects in the commands resulting in maximum tracking errors of 13 cm as shown in Figure 20.

To correct this tracking error a systematic approach for compensating joint input commands was developed and applied. This method relied on creating input/output relationships between desired joint histories and measured joint angles. An inverse operator was then used to obtain the true servo actuator inputs to achieve the desired joint angle output history. With this compensation, the tracking error was reduced to less than 2.5 cm as shown in Figure 20. This performance is a notable improvement over the other open and closed-loop strategies examined.

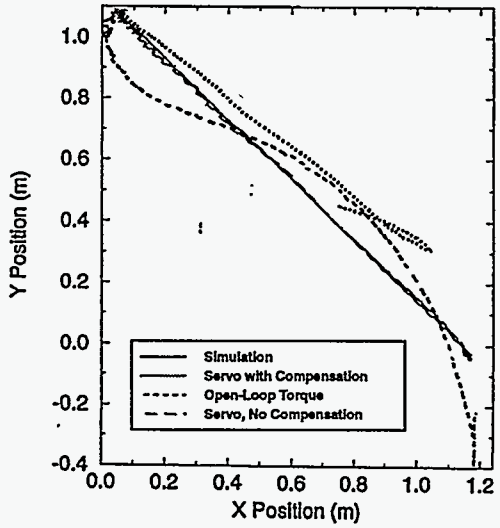

Figure (20): Comparison of Several Control Strategies for Straight Line Tracking

5.4 Sliding Mode Control

In this section augmented sliding mode control[17] is described as it pertains to flexible nonlinear structural systems undergoing large rigid body motion. This method deviates from typical sliding mode control by the incorporation of flexible body generalized accelerations as disturbances during the controller design. It has been demonstrated that this technique not only provides damping of the flexible degrees of freedom, but also results in asymptotic stability of the closed-loop system. For completeness, classical sliding mode control will be reviewed prior to introducing augmented sliding mode control.
Sliding mode control (SMC)[18] was developed in the Soviet Union as a result of research in the more general area of variable structure control. Variable structure control uses a strategy whereby the active control law at any given time is chosen from a previously specified set of control laws, based on the current state of the system. The idea behind SMC is to force the state trajectory of a system to the origin in the error phase hyperplane during two distinct phases. First, the state trajectory proceeds from an initial point in state space to a prescribed sliding surface asymptotically during the *reaching phase*. The sliding surface is constructed such that it contains the origin of the error hyperplane and motion consistent with the sliding surface is asymptotically stable. The second phase, referred to as the *sliding phase*, consists of motion constrained to the sliding surface while moving to the origin of the error hyperplane. The control law for the *reaching phase* can be developed by Lyapunov's direct method. The control law for the *sliding phase* is constructed by enforcing a stationary condition of motion on the sliding surface. However, since the reaching trajectory, in general, will be crossing the sliding surface with nonzero velocity, and to add robustness to modelling errors, a term discontinuous in the sliding surface is added to the sliding control law. This sliding phase control law can also be shown to satisfy the Lyapunov stability condition for the *reaching phase*, resulting in a single control law used for both the *reaching* and *sliding phases.*

Augmented sliding mode control is applicable to nonlinear flexible structural systems undergoing large rigid body translations or rotations where there are fewer actuators than states to be controlled. Control design is similar to classical sliding mode control for the rigid body motion of the system except that the flexible body accelerations are treated as disturbances in the rigid body control design. This formulation specifies a lower bound on control law design parameters to ensure stability while providing damping in the flexible body degrees of freedom considered.

5.4.1 Slewing beam simulation example

Nonlinearities in the system model are due to centrifugal stiffening and gravity[19]. The objective is to rotate the hub of the system to a specified angle while suppressing flexible body vibration. States associated with the rigid body rotation and the first flexible body mode are assumed known. However, the simulation contains the first three flexible body modes. The augmented sliding mode control technique described above is used along with sliding mode control and Proportional-Integral-Derivative (PID) control. The control law design parameters for each controller were chosen using a numerical constrained optimization code ensuring an even comparison between controllers.

The simulated test system is shown in Figure 21. The hub is assumed to have negligible radius. The (X, Y, Z) inertial coordinate

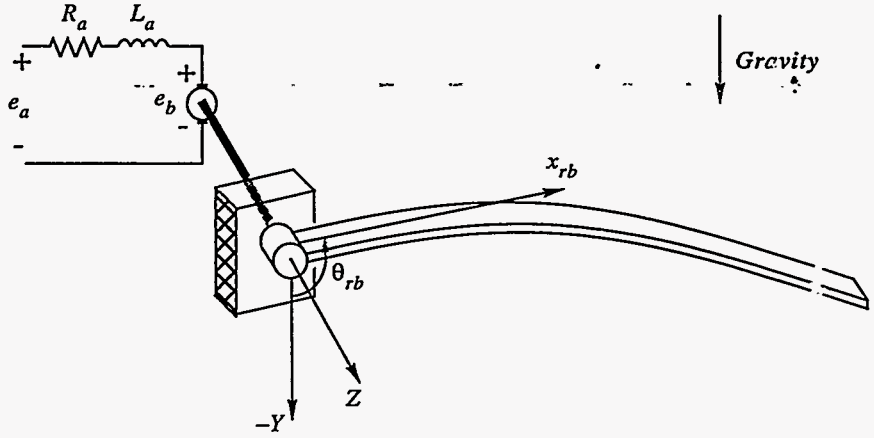

Figure (21): Motor/Beam System.

system is oriented such that when the system is at rest, the beam lies along the X axis. The $(x, y, z)_{rb}$ axes are fixed to the hub rotating about the Z axis with angular velocity $\dot{\theta}_{rb}$. The Z and z_{rb} axes are collinear, and the x_{rb} axis is along the tangent line of the beam at the hub. The armature controlled DC motor has negligible armature inductance and a gear ratio between the motor and the beam of N_g.
The physical parameters of the beam and the motor are the same as used by Juang[20] with the addition of 0.2 % material damping. Figure 22 and Figure 23 show step responses of the hub angle and tip deflection for each of the controllers considered, respectively. Experimental verification of these results is currently in progress using the Sandia Multiple Flexible Link Robot Testbed.

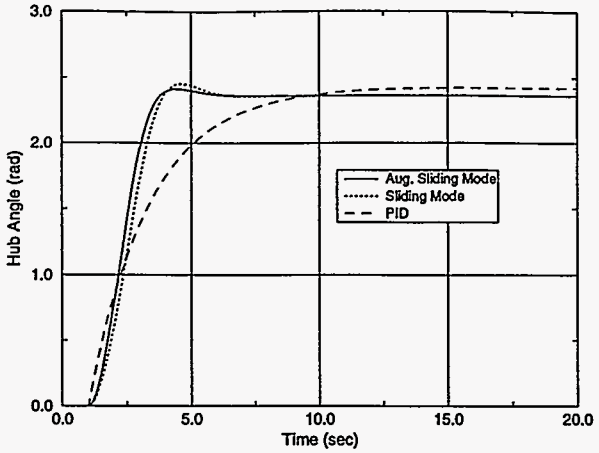

Figure (22): Hub Angle During 2.356 radian Slew.

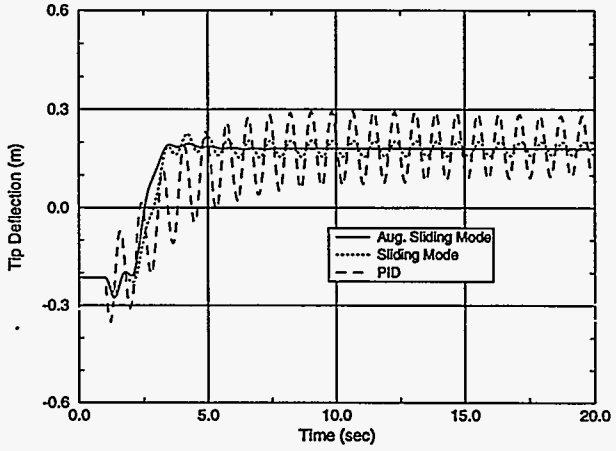

Figure (23): Tip Deflection Relative to Rotating Reference Frame during 2.356 radian Slew.

6.0 SUMMARY

Sandia National Laboratories performs R&D in structural dynamics and vibration control problems for precision applications in weapon systems. Over the last decade these efforts have moved into the areas of active vibration control and "smart" structures and material systems. In addition to weapon product development, Sandia has applied these "smart"techniques to advanced agile manufacturing technology for defense and industrial applications. After giving a brief description of the structural dynamics modeling and analysis process , this paper focused on recent and on-going vibration control projects at Sandia associated with advanced lithography machines for microelectronics manufacturing, milling machines, and flexible robotic control technologies

Other projects at Sandia that involve vibration control of precision manufacturing include active chatter control on grinding machines, vibration control on next generation machine tools using Stewart-like platforms, system identification for the automotive and tire industry, and solar reflector shape control using shape memory alloys.

7.0 ACKNOWLEDGMENTS

This work performed at Sandia National Laboratories is supported by the U.S. Department of Energy under contract DE-AC04-94AL85000. The support of the principal investigators who performed the work that this paper has briefly summarized is greatly appreciated. These principal investigators include Jim Redmond, Gordon Parker, Dan Segalman, Clark Dohrmann, Rick Eisler, Jeff Dohner, and Rush Robbinett.

REFERENCES

1. J. Redmond, J. Dohner, G. Parker and G. Reese, "Segregated Rigid and Flexible Body Controls for a Photolithography Positioning System", Fifth International Conference on Adaptive Structures, Sendai, Japan, December 5-7, 1994.

2. D. Segalman, R. Kipp, D. Gregory, "Passive Damping to Enhance Active Positioning of a Prototype Lithography Platen", 1995 North American Conference on Smart Structures and Materials, Passive Damping Session, San Diego, CA.

3. Redmond, J.M., "Modeling/Simulation for Vibration Control of High Speed Milling Machines", Sandia National Laboratories Memo, Nov. 1, 1994.

4. Jemielniak, K. and Widota, A., "Numerical Simulation of Non-Linear Chatter Vibration in Turning," *International Journal of Machine Tools Manufacturing*, Vol. 29, No. 2, pp. 239-247, 1989.

5. Smith, S. and Tlusty, J., "Update on High-Speed Milling Dynamics," *Symposium on Integrated Intelligent Manufacturing Analysis and Synthesis*, PED Vol. 25, pp. 153-165, 1987.

6. Smith, S. and Tlusty, J., "NC Programming for Quality in Milling," *16th NAMRC*, pp. 279-286, 1988.

7. Smith, S. and Delio, T., "Sensor-Based Chatter Detection and Avoidance by Spindle Speed Selection," *Journal of Dynamic Systems, Measurement, and Control*, Vol. 114, pp. 486-492, 1992.

8. Smith, S. and Tlusty, J., "An Overview of Modeling and Simulation of the Milling Process," *Journal of Engineering for Industry*, Vol. 113, pp. 169-175.

9. Tlusty, J. and Ismail, F., "Special Aspects of Chatter in Milling," *Journal of Vibration, Acoustics, Stress, and Reliability in Design*, Vol. 105, pp. 25-32.

10. Juang, J.N., and Pappa, R.S., "An Eigensystem Realization Algorithm for Modal Parameter Identification and Model Reduction," *Journal of Guidance*, Vol. 8, No. 5, pp. 620-627, 1985.

11. Dohner, J.L., "The Eigensystem Realization Algorithm and the Eigensystem Realization Algorithm with Data Correlation: Theory and Application," Sandia Technical Memorandum, July 27, 1994.

12. Petterson, B.M. and Robinett, R.D., 1991, "Model-Based Damping of Coupled Horizontal and Vertical Oscillations in a Flexible Rod," *Journal of Intelligent and Robotic Systems*, Vol. 4, pp. 285-299.

13. Parker, G.G., Eisler, R., Phelan, J., and Robinett, R., "Input Shaping of Vibration-Damped Slewing of a Flexible Beam Using a Heavy-Lift Hydraulic Robot", American Control Conference, Baltimore, MD, 1994.

14. Parker, G.G., Petterson, B.M., Dohrmann, C.R., Robinett, R.D., "Vibration Suppression of Fixed-Time Jib Crane Maneuvers," 1995 North American Conference on Smart Structures and Materials, Passive Damping Session, San Diego, CA.

15. Dohrmann, C.R. and Robinett, R.D., "Robot Trajectory Planning via Dynamic Programming", Fifth International Symposium on Robotics and Manufacturing, 1994.

16. Parker, G.G., Eisler, G.R., Feddema, J.T., "Optimal Trajectories for Flexible-Link Manipulator Slewing Using Recursive Quadratic Programming: Experimental Verification", Fifth International Symposium on Robotics and Manufacturing, Aug, 1994.

17. Parker, G.G., 1994, "*Control Techniques for Multibody Flexible Structures Modelled by a Method of Quadratic Modes*", Ph.D. Dissertation, State University of New York at Buffalo.

18. Utkin, V.I., 1977, "Variable Structure Systems with Sliding Modes", *IEEE Transactions on Automatic Control*, Vol. 22, No. 2, pp. 212-222.

19. Garcia, E., 1989, Ph.D. Dissertation, Dept. of Mechanical and Aerospace Engineering, State Univ. of New York at Buffalo.

20. Juang, J.N., Horta, L.G. and Robertshaw, H.H., 1986, "A Slewing Control Experiment for Flexible Structures", *AIAA Journal of Guidance, Control and Dynamics*, Vol. 9, No. 5, pp. 599-607.

DISCLAIMER